March 2002

Crystalline Structure and Dielectric Properties of $Li_{1+x-y}Nb_{1-x-3y}Ti_{x+4y}O_3$ *M*-Phase Solid Solutions

Albina Y. Borisevich
University of Pennsylvania

Peter K. Davies
University of Pennsylvania, davies@lrsm.upenn.edu

Crystalline Structure and Dielectric Properties of $Li_{1+x-y}Nb_{1-x-3y}Ti_{x+4y}O_3$ *M*-Phase Solid Solutions

Abstract

The structure and dielectric properties of the so-called *M*-phase solid solutions in the Li_2O-Nb_2O_5-TiO_2 system have been investigated. Detailed studies of the lattice parameters of these phases agree well with structure models based on intergrowths of $LiNbO_3$ slabs with a titanium-rich corundum-type layer. The relative permittivity ranges from ~80 to ~55; microwave quality factors increase with the titanium content, reaching values of $Q \times f = 9000$ at 6 GHz. The temperature coefficient of the resonant frequency changes sign within the solid solution region, thus permitting tunability to a zero value. All the compositions can be sintered to high density at temperatures $\leq 1100^{\circ}C$.

journal

J. Am. Ceram. Soc., **85** [3] 573–78 (2002)

Crystalline Structure and Dielectric Properties of $Li_{1+x-y}Nb_{1-x-3y}Ti_{x+4y}O_3$ *M*-Phase Solid Solutions

Albina Y. Borisevich and Peter K. Davies*

Department of Materials Science and Engineering, University of Pennsylvania, Philadelphia, Pennsylvania 19104-6272

The structure and dielectric properties of the so-called *M*-phase solid solutions in the Li_2O–Nb_2O_5–TiO_2 system have been investigated. Detailed studies of the lattice parameters of these phases agree well with structure models based on intergrowths of $LiNbO_3$ slabs with a titanium-rich corundum-type layer. The relative permittivity ranges from ~80 to ~55; microwave quality factors increase with the titanium content, reaching values of $Q \times f = 9000$ at 6 GHz. The temperature coefficient of the resonant frequency changes sign within the solid solution region, thus permitting tunability to a zero value. All the compositions can be sintered to high density at temperatures ≤1100°C.

I. Introduction

THE rapid growth of the wireless communication industry has created a high demand for microwave ceramic components. In addition to the materials requirements of high dielectric constant (ε_r), low dielectric loss (tan $\delta = 1/Q$), and a zero temperature coefficient of resonant frequency (τ_f), low cost of individual components and processing is a critical requirement for commercial application. Because most contemporary commercial resonator materials have processing temperatures of ≥1300°C,[1] there is considerable interest in the development of new materials with low sintering temperatures. One favored approach has involved investigations of the effect of eutectic or glassforming additives on the properties of established microwave materials. Another approach involves studies of new systems with lower melting points.[2] This article focuses on the latter method and investigates the so-called *M*-phase solid solutions, $Li_{1+x-y}Nb_{1-x-3y}Ti_{x+4y}O_3$, that are formed in the Li_2O–Nb_2O_5–TiO_2 system. These solid solutions were first described by Villafuerte-Castrejon *et al.*[3] in 1987; however, there have been no previous reports on their dielectric properties.

The Li_2O–Nb_2O_5–TiO_2 system[3] (Fig. 1) contains several compounds with various structure types, such as lithium niobate $LiNbO_3$, rutile TiO_2, ordered rock salt Li_2TiO_3, and spinel $Li_4Ti_5O_{12}$. Of these, $LiNbO_3$ is of special interest because of its ferroelectric and optoelectronic properties. Although the dielectric constant of $LiNbO_3$ at room temperature is high (84),[4] its utility as a microwave dielectric is limited by a large and positive temperature dependence of relative permittivity. A series of so-called *M*-phase solid solutions, which form an extended phase field in the center of the ternary section (see Fig. 1), have structures related to $LiNbO_3$.[3,5] The diffraction patterns of the *M*-phases were interpreted in terms of a $LiNbO_3$-type structure with an incommensurate modulation along the ***c***-axis direction. Neither of the previous studies was able to refine the structures in detail, but two models were proposed. In a first model, developed by Smith and West,[6] the solid solutions were described as incommensurate structures comprised of random intergrowths of $LiNbO_3$-type and rocksalt-type Li_2TiO_3 slabs. This model also predicted that random stacking faults in the anion packing were associated with the interfaces between the two blocks. Hayasi *et al.*[7] used this model to interpret HRTEM images collected from a composition of $Li_{1.111}Nb_{0.889}Ti_{0.111}O_3$, for which they observed a periodic intergrowth structure containing 47-layer slabs of a $LiNbO_3$-type structure separated by single layers of an unknown nature.

In a second model, Roth and Davis[5] proposed the phase field is comprised of a homologous series of commensurate structures, based on ordered intergrowths of $LiNbO_3$ and a spinel-type end member ($Li_4Ti_5O_{12}$). HRTEM investigations of metastable forms of $Li_2Ti_3O_7$[8] revealed the existence of two periodic layered structures that resembled those observed for the *M*-phase systems. These structures contained three- and four-layer slabs of a $LiNbO_3$-type structure separated by single layers of a different nature. Minor additions of Nb_2O_5 were shown to be effective in stabilizing these phases,[9] and the composition of the resulting compound, $Li_{28.5}Ti_{36.5}Nb_{1.1}O_{90}$, was close to the lithium titanate end member $Li_{14}Ti_{19}O_{45}$ identified by Roth.[5] Recently, this structure was solved using Rietveld analysis[10] and was found to be commensurate with blocks of four-layer $LiNbO_3$-type slabs separated by a single $Ti_2O_3^{2+}$ corundum-type layer, with the charged layer being compensated by Ti^{4+}/Nb^{5+} substitution in the $LiNbO_3$ slabs. If it is assumed that this composition is the true end member of the *M*-phase system, no oxygen stacking faults are expected at the interface between the corundum layer and $LiNbO_3$ slab.

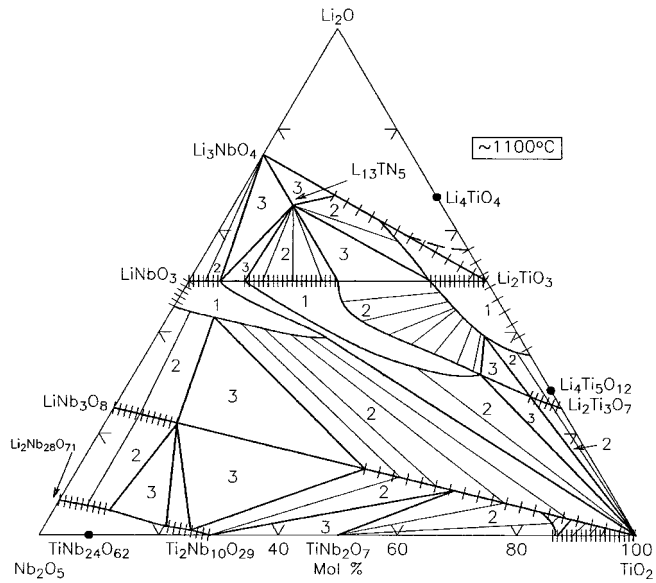

Fig. 1. Phase equilibria in the Li_2O–TiO_2–Nb_2O_5 system (taken from Ref. 5, original work in Ref. 3).

R. S. Roth—contributing editor

Manuscript No. 188128. Received November 27, 2000; approved April 2, 2001.
Supported by the National Science Foundation under Grant Nos. DMR98–09035 and INT98–11609, and in part by MRSEC Shared Experimental Facilities under Grant No. DMR 96–32598.

*Member, American Ceramic Society.

The goal of this study was to reinvestigate the structure and compositional range of the $Li_{1+x-y}Nb_{1-x-3y}Ti_{x+4y}O_3$ *M*-phase solid solutions and examine the suitability of their dielectric properties for possible microwave applications. Because they could be readily sintered to high density at temperatures ≤1100°C, these systems also offered promise as low-sintering dielectrics.

II. Experimental Procedure

Samples of the *M*-phase solid solutions with $Li_{1+x-y}Nb_{1-x-3y}Ti_{x+4y}O_3$ were synthesized from dried Li_2CO_3 (99.0%, J. T. Baker Chemical Co., Phillipsburg, NJ), Nb_2O_5 (99.95%, Cerac, Inc., Milwaukee, WI), and TiO_2 (99.9%, Cerac) powders. After they were mixed under acetone, the powders were preannealed at 700°C to drive off CO_2, then reground and annealed in platinum crucibles at 1100°C for 10 h with subsequent ball-milling in ethanol. The annealing and ball-milling step was repeated until the XRD pattern of the resulting powder was free of impurity peaks (two to seven times, depending on the composition). Pellets were formed from the ball-milled powder, isostatically pressed at 80 000 psi (550 MPa), and sintered at 1100°C for 1 h in platinum envelopes to prevent lithium loss.

XRD patterns were collected (Model DMaxB diffractometer, Rigaku Co., Tokyo, Japan) using Cu*K*α radiation generated at 45 kV and 30 mA. Data for lattice parameter refinements were collected at slow scan speeds; the use of an internal standard consistently resulted in no adjustment to the registered values and was then considered unnecessary. Peak positions for the lattice parameter refinements were determined using Lorentzian fit. Hexagonal cell parameters and an incommensurate parameter δ were refined simultaneously on an array of 22 to 27 fundamental reflections using a specially written program exploiting modified least-squares methods.

The relative permittivity (ε_r) and dielectric loss tangent (tan δ) were measured in the 100 Hz to 1 MHz frequency range from –100° to 200°C using the parallel-plate method (Model HP 4284A precision LCR meter, Hewlett–Packard, Palo Alto, CA, and a Model 9920 environmental chamber, Delta Design, San Diego, CA). The temperature coefficient of the relative permittivity (τ_ε) was calculated for –20° to 80°C from linear fits of the permittivity data. Reproducibility was controlled by using at least two separately prepared samples for each composition. Microwave measurements were performed using the cavity reflection method (Model HP 8719C network analyzer, Hewwlett–Packard). Ceramics with a height to diameter ratio of ~0.4 were placed into a gold-plated resonant cavity, and their permittivities and *Q* values were calculated at the resonant conditions from the S_{11} reflection coefficients. τ_f values were determined in the temperature range 0°–80°C by inserting the test cavities into a temperature-controlled chamber. Polarization measurements were performed using a ferroelectric test system (Model RT66A, Radiant Technologies, Albuquerque, NM) in virtual ground mode.

III. Results

Twenty samples with compositions inside and adjacent to the previously identified *M*-phase field were prepared and examined using XRD. Using the notation reported by Smith and West,[6] the composition of the *M*-phase solid solutions was represented as $Li_{1+x-y}Nb_{1-x-3y}Ti_{x+4y}O_3$, where *y* represents a site-balanced substitution ($Li^{+} + 3Nb^{5+} = 4Ti^{4+}$) and *x* a site-imbalanced substitution ($Nb^{5+} = Li^{+} + Ti^{4+}$). For $y = 0$, single *M*-phase solid solutions had been reported to form for $0.1 \le x \le 0.3$ (see Fig. 1); in this work Li_2TiO_3 impurity phases could not be eliminated for the higher values of *x*, and homogeneous samples could be prepared only for $0.1 \le x \le 0.2$. For $y = 0.025$, single-phase samples were obtained for $0.1 \le x \le 0.15$; when $0.05 \le y \le 0.15$, solid solutions were formed for $0.05 \le x \le 0.15$. The solubility limit was observed at $y = 0.175$, $x = 0.1$, which is in good agreement with the data of Smith and West.[6]

The diffraction patterns collected from the *M*-phase samples were similar to those reported previously.[3,5,6] Indexing of the patterns was conducted using fractional *l* Miller indexes and an incommensurate parameter δ using both of the schemes proposed in the literature. In the scheme proposed by Smith and West,[6] δ is defined as $c_{subcell}/c_{supercell}$, and the peaks with $l = 0$, 4 remain unsplit, those with $l = 2$ are split with $l \pm (2n + 1)\delta$, and those with $l = 3$, 6 are split with $l \pm 2n\delta$. Attempts to index our experimental data within this scheme were unsuccessful. An alternate indexing scheme suggested by Roth and Davis[5] utilizes rhombohedral extinction rules with a symmetric splitting for $l = 3p(l \pm 3n\delta)$, and asymmetric splitting for $l = 3p + 1$ $((l + \delta) \pm 3n\delta)$ and $l = 3p + 2$ $((l - \delta) \pm 3n\delta)$, where δ is now defined as $2c_{subcell}/c_{supercell}$. This scheme was found to give an excellent fit to the experimental data; an example of an indexed pattern is given in Table I.

The quantity $c_{supercell}/c_{subcell}$ $(= 2/\delta)$ in Roth's indexing scheme can be interpreted as the average number of layers $\langle n \rangle$ in the repeating block of each composition. The refined cell parameters, the incommensurate parameters δ, and the mean block length $\langle n \rangle$ for all the single-phase compositions are summarized in Table II. Although the subcell parameters *a* and *c* show small (~1%) variations across the phase field, these changes exhibit well-defined compositional trends and are discussed later. δ and, hence, $\langle n \rangle$ show a strong and systematic variation with *x* and *y*.

The dielectric properties of dense (≥93%) ceramics of the single-phase powders were measured at frequencies from 100 Hz to 1 MHz between –100° and 200°C. The results for ε_r and the temperature coefficient of the capacitance at 1 MHz are listed in Table III. The values for ε_r listed in Table III were corrected for the relative density and represent the average of two or three separately prepared samples of each composition. The observed ε_r values were quite high and ranged from 84 ($x = 0.15$, $y = 0$) to 61 ($x = 0.1$, $y = 0.175$). A graphical compilation of the dielectric data presented in Fig. 2 demonstrates that ε_r exhibits well-defined compositional trends and generally decreases with increasing *x* and *y*. For all samples, the 1 MHz ε_r shows a linear dependence with temperature (Fig. 3), thus justifying the method of determining τ_ε using a linear fit. Table III shows that τ_ε also varies strongly with composition, ranging from ~200 to ~–100 ppm/K for $x = 0.1$, $y = 0.0$ to $x = 0.1$, $y = 0.175$. In the middle of the phase field, τ_ε changes sign, and many compositions exhibit low values. The

Table I. Indexed Powder XRD Pattern for $x = 0.15$, $y = 0.075$

$2\theta_{obs}$	$2\theta_{calc}$	*I*	*h*	*k*	*l*
20.01	20.02	1	0	1	2 − 10δ
20.51	20.53	2	0	1	2 − 7δ
21.57	21.60	11	0	1	2 − 4δ
23.14	23.15	100	0	1	2 − δ
25.10	25.10	48	0	1	2 + 2δ
27.38	27.37	4	0	1	2 + 5δ
33.63	33.63	67	1	0	4 + δ
34.98	34.98	36	1	1	0
38.81	38.80	1	0	0	6
40.15	40.17	17	1	1	3
41.51	41.48	1	2	0	2 − 4δ
42.40	42.37	7	2	0	2 − δ
43.55	43.54	5	2	0	2 + 2δ
49.32	49.31	21	0	2	4 + δ
50.46	50.45	2	1	1	6 − 3δ
53.24	53.23	28	1	1	6
55.34	55.36	2	1	2	2 − 4δ
56.06	56.07	10	1	2	2 − δ
57.04	57.03	5	1	2	2 + 2δ
59.28	59.26	9	0	1	8 + 2δ
61.88	61.88	14	1	2	4 + δ
62.73	62.74	12	3	0	0
70.70	70.70	4	2	0	8 + 2δ
72.27	72.28	5	1	0	10 + δ
73.89	73.90	3	2	2	0

Table II. Lattice Parameters and Block Lengths for Various *M*-Phase Compositions

x	*y*	*a* (Å)	*c* (Å)	δ	⟨*n*⟩
0.1	0	5.148(5)	13.848(3)	0.040(2)	49.76
0.15	0	5.152(6)	13.848(4)	0.055(8)	35.87
0.2	0	5.148(0)	13.858(0)	0.074(4)	26.90
0.1	0.025	5.144(3)	13.866(1)	0.089(1)	22.44
0.15	0.025	5.139(3)	13.878(3)	0.119(3)	16.76
0.05	0.05	5.134(3)	13.868(6)	0.107(5)	18.61
0.1	0.05	5.132(4)	13.876(2)	0.127(7)	15.66
0.05	0.075	5.131(5)	13.880(5)	0.119(2)	16.77
0.1	0.075	5.130(0)	13.904(2)	0.167(3)	11.95
0.15	0.075	5.126(0)	13.912(8)	0.180(9)	11.05
0.05	0.1	5.116(2)	13.874(7)	0.131(4)	15.22
0.1	0.1	5.125(0)	13.924(8)	0.200(3)	9.98
0.15	0.1	5.117(7)	13.927(5)	0.218(4)	9.16
0.1	0.125	5.110(6)	13.919(9)	0.221(5)	9.03
0.1	0.15	5.099(7)	13.913(3)	0.223(9)	8.93
0.1	0.175	5.099(7)	13.901(3)	0.226(1)	8.85

systematic variation from positive to negative values of τ_ε demonstrates that this system is highly tunable.

tan δ, observed at 1 MHz, was low ($\sim 10^{-4}$) for all the compositions except those close to the $LiNbO_3$–Li_2TiO_3 join. For many of the samples, the value registered was negative, suggesting that the precision of the measurement was not high enough to determine the actual loss. Data for the microwave dielectric properties were collected for selected samples of the *M*-phase solid solutions and are presented in Table IV. The values of ε_r (78–55) at gigahertz frequencies were in good agreement with those observed at 1 MHz. τ_f also exhibited a tunability to zero. The *Q* values, which are the reciprocal of δ, increase with the titanium content, reaching a $Q \times f = 9000$ (at 6 GHz) for the sample with $x = 0.1$, $y = 0.175$.

Because $LiNbO_3$ is a well-known ferroelectric with a very high Curie temperature and one of the highest values of remnant polarization,[4] it was of interest to examine if a collective ferroelectric response was retained in any of the *M*-phases, particularly those with the longest block lengths. Polarization versus field data was collected for all the single-phase samples. Although the vast majority demonstrated purely paraelectric behavior, some samples did exhibit evidence for very weak ferroelectricity. However, this phenomenon was subsequently found to result from a low volume fraction of nanosized inclusions of $LiNbO_3$ that were undetectable using XRD but observable by piezoresponse imaging.[11] Therefore, it was concluded that, in the temperature range investigated, all the *M*-phase compositions were paraelectric.

Table III. Dielectric Properties of *M*-Phase Samples at 1 MHz

x	*y*	ε_r, 25°C	τ_ε (ppm/K)
0.1	0	74.6	+197
0.15	0	83.5	+217
0.2	0	74.0	+208
0.15	0.025	72.88	+115
0.05	0.05	73.8	+63
0.1	0.05	71.7	+51
0.05	0.075	64.4	+55
0.1	0.075	72.4	+29
0.15	0.075	66.6	−28
0.05	0.1	64.8	+39
0.1	0.1	69.7	−45
0.15	0.1	63.8	−88
0.1	0.125	64.3	−94
0.1	0.15	60.8	−95
0.1	0.175	60.7	−127

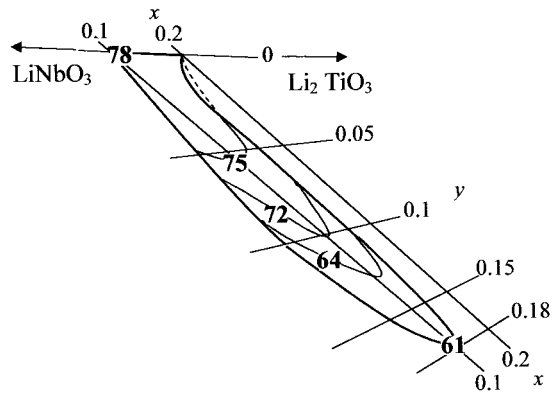

Fig. 2. Variation of the relative permittivity of the *M*-phase system as a function of composition.

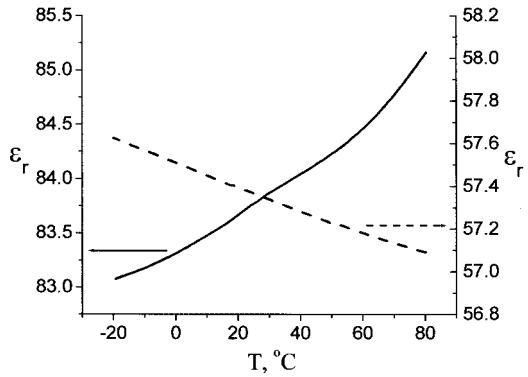

Fig. 3. Variation in the relative permittivity (ε_r) with temperature for (—) $x = 0.15$, $y = 0$ and (– – –) $x = 0.1$, $y = 0.15$.

IV. Discussion

Because most of the observed characteristics of the *M*-phase system vary with composition, this discussion begins by evaluating the various models for the structure of these solid solutions. All the models presented thus far in the literature agree that the structure of this system is comprised of intergrowths of $LiNbO_3$-type slabs with a length that depends on the composition, separated by layers of a different structure type. $\langle n \rangle$ in the repeating block determined from the cell refinements varied from ~50 to ~9. Although the noninteger values listed in Table II imply an incommensurate repeat along *c*, we believe that the observed $\langle n \rangle$ represents an averaged value of two or more commensurate repeats. Support for this interpretation was obtained from investigations of the system using electron diffraction and HRTEM where, for example, a sample with $x = 0.2$, $y = 0.0$ (with an XRD refined $\langle n \rangle = 26.9$)

Table IV. Dielectric Properties of Selected *M*-Phase Samples at Microwave Frequencies

x	*y*	f_{res} (GHz)	ε_r, 25°C	τ_f (ppm/K)	*Q*	$Q \times f$ (GHz)
0.15	0	5.321	76.21	−62	187	997
0.05	0.05	5.206	77.76	−42	419	2184
0.1	0.05	6.009	62.38	−53	657	3949
0.1	0.075	5.917	64.04	−15	779	4612
0.05	0.1	6.312	58.45	−31	987	6233
0.1	0.1	5.660	64.79	+8	1128	6385
0.1	0.125	6.052	59.16	+22	1250	7565
0.1	0.15	6.029	56.19	+15	1384	8345
0.1	0.175	6.153	54.88	+28	1446	8896

was found to be comprised of two intergrowth structures with 26- and 28-layer repeats. The details of the microscopy studies are reported elsewhere.[12]

$<n>$ in the repeating block of the intergrowth structure is a highly nonlinear function of the compositional coordinates, as illustrated in Fig. 4, for the $x = 0.1$ and $x = 0.15$ series of samples. This dependence has a hyperbolic shape that can be easily derived for any structure with two types of layers of fixed composition. However, the composition of the $LiNbO_3$-type slabs in the *M*-phase systems is not fixed, and an explicit expression for the variation of $<n>$ with composition is not possible without additional information. To gain additional insight into the nature of the structure and the composition of the $LiNbO_3$ slabs and the second intergrowth layer, an alternate approach to reproducing the dependence of $<n>$ on compositions was developed. The *a* parameter of the *M*-phases shows a well-defined linear dependence on *y* (Fig. 5), but exhibits very little variation with *x*. Because the superstructure forms along the *c* direction, it is reasonable to suggest that *a* is not affected by the block length and is primarily determined by the effective radii of the ions on the lithium and niobium sites within the $LiNbO_3$-type slabs. Because there are two independent sets of data, namely for the *a* parameter and for $<n>$, their mutual agreement can be checked for different models of the structure. The first model that was utilized in this analysis was based on the work of Bordet *et al.*,[10] where the layers separating the $LiNbO_3$ slabs are assumed to have the stoichiometry $Ti_2O_3^{2+}$. The [Ti] to [Nb] ratio was estimated from the value of the *a* parameter using tabulated ionic radii[13] (without referral to the actual compositional data) and compared with the value of the [Ti] to [Nb] ratio expected for a given composition with the observed block lengths.

To avoid using bulk composition data, basic chemical concepts, such as charge balance, were utilized. If it is assumed that the impact of the charged $Ti_2O_3^{2+}$ layers on the charge balance within the $LiNbO_3$ slab is insignificant, then

$$[Li^+] + 4[Ti^{4+}] + 5[Nb^{5+}] = 3[O^{2-}] = 6 \quad (1)$$

where $[X^q]$ represents the concentration of a given ion per formula unit within the $LiNbO_3$ slab. The site balance in $LiNbO_3$ is given by

$$[Li^+] + [Nb^{5+}] + [Ti^{4+}] = 2 + \alpha \quad (2)$$

where α is the site off-stoichiometry. Simple geometric derivation results in the following expression for the *a* parameter of the structure:

$$a = \left(\frac{3}{2}\right)^{1/2} (R_{Li} + R_{Nb} + 2r_O) \quad (3)$$

where R_{Li} and R_{Nb} represent the effective radii on the respective sites and $r_O = 1.40$ Å. Expressing the effective site radii as linear combinations of the individual ionic radii, and assuming that

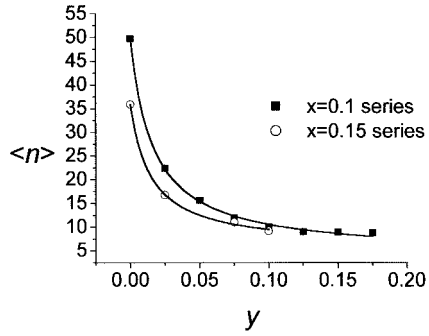

Fig. 4. Mean block length ($<n>$) versus composition for $x = 0.1$ and $x = 0.15$ series.

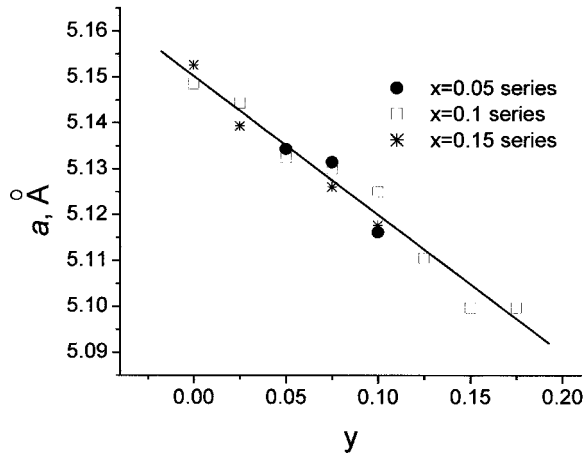

Fig. 5. Variation of the *a* parameter versus composition.

off-stoichiometry is predominantly accommodated by Li^+ ions, yields the following expression:

$$a = \left(\frac{3}{2}\right)^{1/2} (r_{Li}([Li^+] - \alpha) + r_{Nb}[Nb^{5+}] + r_{Ti}[Ti^{4+}] + 2r_O) \quad (4)$$

where r_X represents the octahedral ionic radii of the corresponding ions.

Using these equations, an expression for $k = [Ti^{4+}]/[Nb^{5+}]$ can be obtained as a function of *a* and α:

$$k = \frac{r_{Nb}(4 - \alpha) + r_{Li}(4 + \alpha) + 8r_O - 4\left(\frac{2}{3}\right)^{1/2} a}{6^{1/2}a - r_{Ti}(4 - \alpha) - r_{Li}(2 + \alpha) - 6r_O} \quad (5)$$

For the $x = 0.1$ series of samples, where $\alpha < 0.1$ for all compositions, α can be assumed to be approximately zero, and Eq. (5) simplifies to

$$k_0 = \frac{4r_{Nb} + 4r_{Li} + 8r_O - 4\left(\frac{2}{3}\right)^{1/2} a}{6^{1/2}a - 4r_{Ti} - 2r_{Li} - 6r_O} \quad (6)$$

This estimate for *k* can now be compared with that expected for a composition $Li_{1+x-y}Nb_{1-x-3y}Ti_{x+4y}O_3$ with a mean block length $<n>$ when the extra layer is assumed to be $Ti_2O_3^{2+}$.[10] In this case

$$k = \frac{\langle n\rangle(x + 4y) - 2}{\langle n\rangle(1 - x - 3y)} \quad (7)$$

For this model, the *k* values calculated from Eqs. (6) and (7) show remarkable agreement (see Fig. 6). If the composition of the additional layer separating the $LiNbO_3$ slabs is instead assumed to be Li_2TiO_3,[6] then the analogous formula for *k* is

$$k = \frac{\langle n\rangle(x + 4y) - 1}{\langle n\rangle(1 - x - 3y)} \quad (8)$$

In this case, the agreement is not as good (Fig. 6). Therefore, we believe that our X-ray data provide significant support for the model of the *M*-phase described by Bordet *et al.*[10]

The *c* subcell parameter is affected by the site composition and the block length and has an unusual dependence on composition, increasing up to $y = 0.1$ and then decreasing for higher values of *y* (Fig. 7). Smith and West[6] reported a different *c* parameter dependence that can be attributed to the different indexing scheme utilized in that work. The variation of *c* also can be explained if the compound studied by Bordet *et al.*[10] is assumed to be the end member for the *M*-phase solid solutions. In this model, the charged $Ti_2O_3^{2+}$ layers and the interlayer Li^+ cations can be expected to

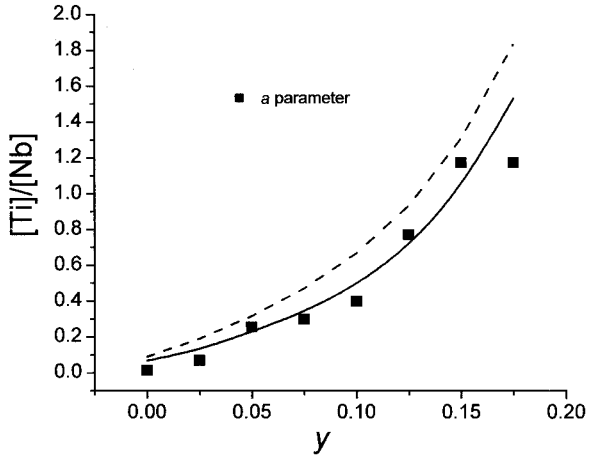

Fig. 6. [Ti] to [Nb] ratio in $LiNbO_3$-type block for $x = 0.1$ series from *a* parameter (Eq. (6)), for (—) $Ti_2O_3^{2+}$ extra layer (Eq. (7)) and for (– – –) Li_2TiO_3 extra layer (Eq. (8)).

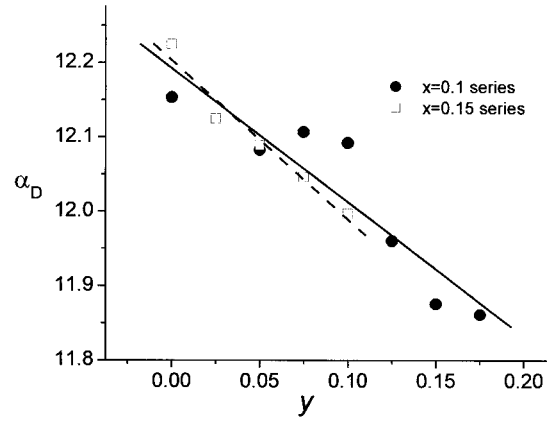

Fig. 8. Dielectric polarizability (α_D) as a function of composition.

contribute to the expansion of the lattice along the *c* direction. The level of this contribution to the cell parameter should increase as the block length decreases (higher *y*). However, the increasing levels of titanium decrease the effective radii within the $LiNbO_3$ slabs and favor a decrease in *c*. For low *y*, where the rate of change of $<n>$ with *y* is large, the first effect dominates, while, for high *y* values, where $<n>$ remains almost constant, apparently the second effect predominates. Further support for these structure models was obtained using HRTEM,[12] where the layers separating the $LiNbO_3$ slabs were found to have a structure related to corundum rather than to rocksalt or spinel.

Consistent with the systematic variations in their structure, the dielectric properties of the *M*-phases also show well-defined changes across the system. The permittivities are high and range from 84 for $x = 0.15$, $y = 0$, to 61 for $x = 0.1$, $y = 0.175$. The effect of the changes in composition on the dielectric permittivities can be analyzed using the dielectric polarizability (α_D), which eliminates the effect of the alterations in unit-cell volume across the solid-solution field. The polarizabilities were calculated using the Clausius–Mossotti equation (where $\alpha_D = (3/4)\pi V_m(\varepsilon_r - 1)/(\varepsilon_r + 2)$, where V_m is the molar volume and $V_m = V_{unitcell}/Z$, and where *Z* is the number of formula units per cell). The plots of the polarizability for selected series of samples (Fig. 8) reveal a linear decrease in α_D with an increase in *y*. The decrease in the polarizability is consistent with empirical estimates of α_D obtained using the ion additivity rule and the ionic dielectric polarizabilities reported by Shannon.[14] The linear dependence of α_D on *y* implies that the permittivities of the *M*-phases are primarily determined by their bulk composition rather than by the lengths of the $LiNbO_3$ slabs or other structural characteristics. Moreover, the absence of anomalous variations in α_D and of ferroelectric behavior, even in compositions with the largest block lengths, suggests that the introduction of the corundum-type layer disrupts the long-range correlations of the lithium displacements that produce ferroelectric behavior in pure $LiNbO_3$.[15]

τ_ε values at 1 MHz also exhibit systematic changes with composition. Large positive values are observed for the lowest values of *y* (Fig. 9), while samples with the highest titanium concentrations exhibit a large and negative τ_ε. The systematic dependence of τ_ε on *y* is illustrated in Fig. 9 for the $x = 0.1$ and 0.15 series of samples. The change in sign of τ_ε produces a zero coefficient for several compositions in the middle of the system. The microwave τ_f values follow a similar trend, and, for example, a zero τ_f can be expected for $x = 0.1$, $y \approx 0.09$.

The microwave quality factors *Q* (Table IV) also exhibit uniform changes with composition and increase in the *y* direction. This change parallels the decrease in permittivity. The highest *Q* value was observed for $x = 0$, $y = 0.175$ ($Q \times f = 9000$), while the zero τ_f composition has $\varepsilon_r \approx 64$, $Q \times f \approx 6400$. All these compositions readily sinter to high density at $T \approx 1100$°C. Further decreases in the sintering temperature are required before these systems can be considered for cofire applications. Currently, we are exploring ways to lower the sintering temperature using chemical substitution schemes. In this regard the introduction of vanadium has been found to be particularly effective and will be reported in a forthcoming publication.[16]

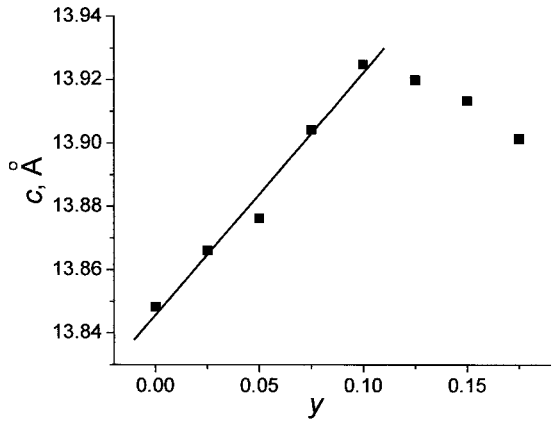

Fig. 7. Variation of the *c* parameter versus composition for the $x = 0.1$ series.

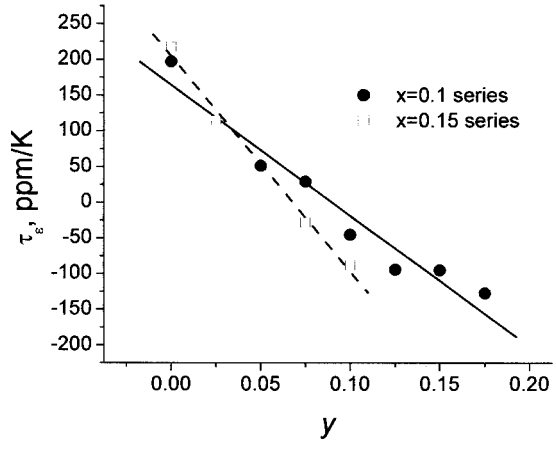

Fig. 9. Temperature coefficient of permittivity (τ_ε) for the $x = 0.1$ and $x = 0.15$ series.

V. Conclusions

The results of investigations of the *M*-phase $Li_{1+x-y}Nb_{1-x-3y}Ti_{x+4y}O_3$ system are consistent with previous reports of the formation of a homologous series of intergrowth structures comprised of $LiNbO_3$-type slabs separated by layers of a different nature. Detailed analyses of the powder XRD data support a model in which the composition of the additional layer has a corundum-type structure and a composition of $Ti_2O_3^{2+}$.

High-density ceramics can be obtained by sintering the solid solutions at 1100°C. All the *M*-phase compositions are paraelectric with dielectric constants ranging from 84 to 61. The temperature coefficient of the relative permittivity changes from positive (+200 ppm/K) to negative (–100 ppm/K) with increasing *y*, and compositions in the middle of the system can be tuned to a zero value. Similar tunability is observed for the temperature coefficient of the resonant frequency measured in the microwave region. The system shows quite good quality factors at microwave frequencies, with the highest value reaching $Q \times f = 9000$ at 6 GHz.

Acknowledgments

The authors thank Dr. M. Valant (Jozef Stefan Institute, Ljubljana) for measurements at microwave frequencies and Dr. D. Lisjak for preliminary studies conducted on this system.

References

[1]P. K. Davies, "Influence of Structural Defects on the Dielectric Properties of Ceramic Microwave Resonators"; pp. 137–51 in Ceramic Transactions, Vol. 53, *Materials and Processes for Wireless Communications*. Edited by T. Negas and H. Ling. American Ceramic Society, Westerville, OH, 1995.

[2]W. Wersing, "Microwave Ceramics for Resonators and Filters," *Curr. Opin. Solid State Mater. Sci*, **1** [5] 715–31 (1996).

[3]M. E. Villafuerte-Castrejon, A. Aragon-Pina, R. Valenzuela, and A. R. West, "Compound and Solid Solution Formation in the System Li_2O–Nb_2O_5–TiO_2," *J. Solid State Chem.*, **71**, 103–108 (1987).

[4] K.-H. Hellwege and A.M. Hellwege (eds.), *Landolt–Bornstein New Series*, Vol. 16a; p. 90. Springer–Verlag, Berlin, Germany, 1981.

[5]R. S. Roth and K. L. Davis, "Incommensurate Solid Solution in TiO_2-Doped $LiNbO_3$ and $LiTaO_3$"; presented at the 89th Annual Meeting of The American Ceramic Society, 1987; and R. S. Roth, *Phase Diagrams for Ceramists*, Vol. XI. Edited by M. A. Clevinger. American Ceramic Society, Westerville, OH, 1995; pp. 231–32.

[6]R. I. Smith and A. R. West, "Characterization of an Incommensurate LiTiNb Oxide," *Mater. Res. Bull.*, **27**, 277–85 (1992).

[7]H. Hayasi, H. Nakano, K. Suzumura, K. Urabe, and A. R. West, "Superstructure in LiTiNb Oxides"; pp. 391–98 in Fourth European Ceramics, Vol. 2, *Basic Science–Developments in Processing of Advanced Ceramics– Part II*. Edited by C. Galassi. Gruppo Editoriale Faenza Editrice, Faenza, Italy, 1995.

[8]J. Zou, F. H. Li, D. Y. Yang, Y. D. Jiang, and K. H. Kuo., "A Transmission Electron Microscopy Study on Metastable Phases in the Li_2O–TiO_2 System," *Philos. Mag. B*, **57** [1] 103–10 (1988).

[9]D. Tsubone and T. Shimizu, "Effect of Nb_2O_5 Addition on the Phase Change in $Li_2Ti_3O_7$," *J. Ceram. Soc. Jpn., Int. Ed.*, **101**, 637–41 (1993).

[10]P. Bordet, C. Bougerol-Chaillout, I. Grey, J. L. Hodeau, and O. Isnard, "Structural Characterization of the Engineered Scavenger Compound, H-$Li_2Ti_3O_7$," *J. Solid State Chem.*, **152**, 546–53 (2000).

[11]A. Y. Borisevich, S. V. Kalinin, D. A. Bonnell, and P. K. Davies, "Analysis of Phase Distributions in the Li_2O–Nb_2O_5–TiO_2 System by Piezoresponse Imaging," *J. Mater. Res.*, **16** [2] 329–32 (2001).

[12]Farber, Levin, Borisevich, Grey, Roth, and Davies, *J. Solid State Chem.*, in review.

[13]R. D. Shannon, "Revised Effective Ionic Radii and Systematic Studies of Interatomic Distances in Halides and Chalcogenides," *Acta Crystallogr., Sect. A: Cryst. Phys. Diffr. Theor. Gen. Crystallogr.*, **32** [5] 751–67 (1976).

[14]R. D. Shannon, "Dielectric Polarizability of Ions in Oxides and Fluorides," *J. Appl. Phys.*, **73** [1] 348–66 (1993).

[15]I. Inbar and R. E. Cohen, "Origin of Ferroelectricity in $LiNbO_3$ and $LiTaO_3$," *Ferroelectrics*, **194,** 83–95 (1997).

[16]A. Borisevich and P. K. Davies, in preparation. □